N-methylmesoporphyrin IX fluorescence as a reporter of strand orientation in guanine quadruplexes

Navin C. Sabharwal[1], Victoria Savikhin[2,3], Joshua R. Turek-Herman[1], John M. Nicoludis,[1,4] Veronika A. Szalai[2], Liliya A. Yatsunyk[1*]*

[1]Department of Chemistry and Biochemistry, Swarthmore College, 500 College Ave., Swarthmore, PA 19081 USA

[2]Center for Nanoscale Science & Technology, National Institute of Standards & Technology, 100 Bureau Drive, Gaithersburg, MD 20899 USA

[3]Current address: Department of Electrical Engineering, Stanford University, Stanford, CA 94305 USA

[4]Current address: Department of Chemistry and Chemical Biology, Harvard University, 12 Oxford St. Cambridge MA 02138, USA

ABBREVIATIONS

GQ, guanine quadruplex DNA; NMM, N-methylmesoporphyrin IX; Tel22, human telomeric DNA repeat model sequence; FL, fluorescence; ssDNA, single-stranded DNA; dsDNA, double-stranded DNA; CT, calf thymus DNA.

ABSTRACT

Guanine quadruplexes (GQ) are four-stranded DNA structures formed by guanine-rich DNA sequences. Formation of GQs inhibits cancer cell growth, but detecting GQs *in vivo* has proved difficult, in part because of GQ structural diversity. Development of GQ-selective fluorescent reporters would enhance our ability to quantify the number and location of GQs, ultimately advancing biological studies of quadruplex relevance and functions. N-methyl mesoporphyrin IX (NMM) interacts selectively with parallel-stranded GQs; in addition, its fluorescence is sensitive to the presence of DNA, making this ligand a possible candidate for a quadruplex probe. We have investigated the effect of DNA secondary structure on NMM fluorescence. We find that NMM fluorescence increases by about 60-fold in the presence of parallel-stranded GQs (IL1,

G4, G8, VEGF, cMyc, and cKit2) and by about 40-fold in the presence of hybrid GQs (cKit1, G4TERT, Bcl-2, Tel22, and 26TelG4). Antiparallel GQs (Tel22, TBA, 26TelG4, and $G_4T_4G_4$, all in sodium ion buffer) cause lower than 10-fold increases in NMM fluorescence. Non-quadruplex DNA structures, such as single-stranded DNA, duplex, or i-motif, induce no change in NMM fluorescence. We conclude that NMM shows promise as a "turn-on" fluorescent probe for detecting quadruplex structures and for differentiating them on the basis of strand orientation.

INTRODUCTION

DNA adopts numerous secondary structures in addition to the canonical Watson-Crick duplex. One example is G-quadruplex (GQ) DNA, a structure formed by π-π stacking of G-quartets, composed of four guanines held together by Hoogsteen hydrogen bonds [1-3] (Fig. 1). To form GQs, a DNA sequence must contain one or more regions of contiguous guanines, typically three or more. Monovalent cations such as sodium, potassium or ammonium, stabilize GQ structures [1, 4]. GQ's can be uni-, bi-, or tetramolecular and adopt parallel, antiparallel, or mixed-hybrid geometry as shown in Fig. 1B, depending on DNA composition, stabilizing cation, and the presence of exogenous ligands [5-9].

G-rich DNA sequences with a propensity to form GQs have been identified throughout the human genome, including in telomeres, oncogenes (*c-MYC, c-MYB, c-FOS, c-ABL*), ribosomal DNA, and immunoglobin switch regions [10-15]. GQs have been proposed to regulate gene expression, chromosomal alignment, recombination, and DNA replication [16]. Conclusive correlation of GQs with cellular processes, however, has proved challenging in part because of the structural diversity exhibited by GQs and also because available probes can induce GQ formation or alter their structures, making it unclear if GQs observed *in vivo* are present prior to probe addition. There is, therefore, a need for new probes to facilitate elucidation of the physiological relevance of GQs.

Selective quadruplex targeting and detection are both important and challenging. A variety of small-molecule probes display fluorescence that is modulated by the presence of GQs; such molecules are highlighted in a recent review [17]. The majority of these probes suffer from low selectivity for GQ vs. dsDNA or toward a specific GQ geometry. It is important to discriminate GQs based on their geometry because it defines the biological roles and functions of GQs, such

as interactions with proteins [18] and drugs [19, 20]. The first example of a "turn-on" fluorescent small molecule dye specific for parallel-stranded, but not antiparallel or mixed-hybrid GQs, was reported recently [21]. This acetylene-bridged purine dimer (APD) interacts with a variety of parallel-stranded GQ structures (c-myc, c-kit1, BCL2, NRAS, TERRA and Src1), displays strong emission in their presence, and exhibits topology-specific staining in agarose gels. Its synthesis, however, is not trivial. In contrast to this small molecule example, Balasubramanian's group reported immunofluorescence detection of GQs [22], thereby improving the ability to map GQs *in vivo*. The need remains for additional GQ selective probes that are either commercially available or easy to prepare and compatible with sensitive *in vivo* detection, primarily by fluorescence microscopy.

   N-methylmesoporphyrin IX, (NMM, Fig. 1C) is highly selective for GQ over ssDNA and ssRNA, dsDNA, triplex DNA, and DNA-RNA hybrids [23, 24]. Some previous work has demonstrated that NMM fluorescence increases in the presence of GQ, but not dsDNA [25, 26]. Recently, NMM has been shown to bind parallel but not antiparallel GQ fold [23, 27]. NMM's potential to discriminate between particular strand orientations of GQs using fluorescence, however, has not been systematically explored. NMM is water-soluble, chemically stable, commercially available, and has excellent optical and fluorescence properties. These attributes combined with NMM's ability to preferentially recognize parallel-stranded GQ structures make it a promising candidate for selective GQ detection. In this work, we applied UV-visible, fluorescence, and circular dichroism spectroscopies to evaluate NMM's potential as a selective fluorescence GQ reporter in the presence of a wide selection of DNA structures.

MATERIALS AND METHODS

Porphyrins, oligonucleotides, and buffers. Disclaimer: Certain commercial entities, equipment, or materials may be identified in this document in order to describe an experimental procedure or concept adequately. Such identification is not intended to imply recommendation or endorsement by the National Institute of Standards and Technology, nor is it intended to imply that the entities, materials, or equipment are necessarily the best available for the purpose.

NMM was purchased from Frontier Scientific (Logan, UT, USA), dissolved in water (resistivity 1.8×10^5 Ω-m) at 0.3 mmol L^{-1} to 1.3 mmol L^{-1}, and stored at 4 °C. NMM stock solutions were freshly diluted with appropriate buffers. NMM concentrations were determined spectrophotometrically using $\varepsilon_{379 \text{ nm}} = 1.45 \times 10^5$ L mol^{-1} cm^{-1} [28]. Tris(hydroxymethyl)amino methane (Tris), boric acid, hydrochloric acid, cacodylic acid, lithium hydroxide (LiOH), tetramethylammonium chloride (TMACl), potassium chloride and magnesium chloride were standard grade reagents and used as received. DNA oligonucleotide sequences used in this work are provided in Table S1. All oligonucleotides were purchased from commercial vendors. Selected sequences were purified by ethanol precipitation as described in the Supporting Information (SI). The following buffers were used in this work:

10 mmol L^{-1} lithium cacodylate, pH 7.2, 5 mmol L^{-1} KCl, 95 mmol L^{-1} LiCl (<u>5K</u>);

10 mmol L^{-1} lithium cacodylate, pH 7.2, 150 mmol L^{-1} KCl (<u>150K</u>);

10 mmol L^{-1} lithium cacodylate, pH 5.8, 5 mmol L^{-1} KCl, 95 mmol L^{-1} LiCl (<u>5K 5.8</u>);

10 mmol L^{-1} lithium cacodylate, pH 7.2, 50 mmol L^{-1} NaCl, 50 mmol L^{-1} LiCl (<u>50Na</u>);

10 mmol L^{-1} lithium cacodylate, pH 7.2, 100 mmol L^{-1} LiCl (<u>100Li</u>);

50 mmol L^{-1} Tris-borate, pH 8.3, 10 mmol L^{-1} KCl, 1 mmol L^{-1} MgCl$_2$ (<u>TB</u>);

50 mmol L^{-1} Tris-borate, pH 8.3, 10 mmol L^{-1} TMACl, 1 mmol L^{-1} MgCl$_2$ (<u>TB-TMACl</u>)

The complete list of buffers can be found in Table S2. TMACl was used in lieu of KCl because it minimizes GQ formation [29].

To induce the formation of the most thermodynamically stable GQ conformations, oligonucleotides were diluted in the desired buffer (with or without added salts) and melted at > 90 °C for 5 min. When required, aliquots of concentrated stock solutions of KCl and/or MgCl$_2$ were mixed into the heated solution, which was then allowed to heat for an additional 5 min, cooled to room temperature over 3 h, and incubated overnight at 4 °C. The i-motif structures

were formed by preparing C-rich sequences in acidic pH [30]. For experiments testing NMM interaction with rigorously single-stranded G-rich sequences, GQ's assembled from IL1 or G4 in TB buffer were treated with 50 mmol L^{-1} LiOH for 30 min after which time the pH was adjusted to neutral by the addition of HCl. The disruption of the quadruplex into single strands was verified using circular dichroism (CD) spectroscopy.

The C1A:C1B duplex was formed in solutions containing 120 µmol L^{-1} of each strand in TB-TMACl buffer. The solution was heated to 95 °C for 10 min, and cooled to room temperature over a period of 3 h. The final duplex was either used as generated or gel-purified on nondenaturing PAGE using TMACl in the running buffer according to literature procedures [31]. A dry sample of calf-thymus (CT) DNA was dissolved in 10 mmol L^{-1} lithium cacodylate, 1 mmol L^{-1} Na_2EDTA to a concentration of approximately 1 mmol L^{-1} (in base pairs) and placed on a nutator for 1 week at 4 °C. Before use, the sample was centrifuged extensively to remove insoluble components and the supernatant was transferred to a clean microcentrifuge tube. Stock DNA and NMM solutions were stored at -80 °C; samples in buffers were stored at either -20 °C or 4 °C depending on the length of time between sample preparation and use.

Concentrations of all DNA oligonucleotide samples were determined spectrophotometrically at room temperature on two types of UV-visible spectrophotometers and are reported as concentration of structural element: GQ, i-motif or duplex. For example, the concentration of a unimolecular GQ is equal to the concentration of oligonucleotide strand, whereas the concentration of a tetramolecular GQ is assumed to be one quarter the oligonucleotide strand concentration. The concentration of genomic CT DNA is reported in base pairs. Extinction coefficients for all single-stranded oligonucleotides are given in Table S1 and were calculated using the nearest-neighbor approximation [32, 33]. Secondary structures of all DNA sequences were verified using CD wavelength scans.

CD spectroscopy. For CD experiments, DNA samples were prepared at 1 µmol L^{-1} to 10 µmol L^{-1} concentrations in desired buffers. Spectra were collected on two types of CD spectropolarimeters, one of which was equipped with a Peltier heating unit (error of ± 0.3 °C). Samples were placed in cylindrical quartz cuvettes (0.1 cm or 0.5 cm pathlengths) or a 1 cm quartz cuvette. Three scans were collected from 350 nm to 220 nm with a 1 nm bandwidth and an average time of 1 s at 25 °C and averaged. CD data were treated as described previously [34].

CD spectra of selected sequences were collected in the presence of a 2-fold excess of NMM to determine its effect on DNA secondary structure. For these experiments, samples were annealed with or without NMM at 90 °C for 10 min, slowly cooled to room temperature and stored at 4 °C overnight before collecting CD scans.

UV-visible and fluorescence spectroscopy. UV-visible spectra for absorption titrations were collected on a spectrophotometer with a Peltier-thermostatted cuvette holder (error of $\pm 0.3\,^{\circ}C$) using a 1 cm quartz cuvette. Spectra were collected in the range of 350 nm to 700 nm at 25 $^{\circ}C$. All experiments were performed at least three times on independently prepared solutions.

Fluorescence experiments were performed on three types of commercially available spectrofluorometers. An NMM solution was prepared in the desired buffer at 1 μmol L^{-1} and its steady-state fluorescence spectrum was measured. Then, to ensure that all NMM was bound to the DNA, DNA was added at 10-fold excess, the sample was equilibrated at room temperature for up to 1 h and its fluorescence spectrum was remeasured. The amount of DNA required to saturate the NMM fluorescence signal was determined from fluorescence titrations, which also were used to obtain binding constants. Titrations of 1 μmol L^{-1} NMM were conducted with G4 (TB), G8 (TB) and VEGF (5K), all of which are parallel-stranded GQs; with antiparallel/mixed-hybrid $G_4T_4G_4$ (5K); and with antiparallel $G_4T_4G_4$ (50Na) and 26TelG4 (50Na). Spectra of NMM in the presence of G4 and G8 were collected in 100 μL volume quartz cuvettes with excitation wavelength of 399 nm; emission wavelength range from 550 nm to 750 nm, slits of 0.5 nm, and integration time of 1 s or 2 s. Spectra of NMM in the presence of VEGF, $G_4T_4G_4$ and 26TelG4 were collected using a 1 cm quartz cuvette and the following parameters: excitation wavelength of 399 nm; emission wavelength range from 550 nm to 700 nm, increment of 1 nm, integration time of 0.5 s; slits of 2 nm, and temperature of 25 °C. Quadruplex $G_4T_4G_4$ in 5K displays tight binding to NMM ($K_a > 10^7$ L mol^{-1}); in this case a solution of only 0.1 μmol L^{-1} NMM was titrated with the quadruplex; data were collected at a single wavelength of 608 nm using 2 points per s and 50 s duration (which corresponds to 100 scans with 0.5 s integration time) to improve S/N. All data were corrected for dilution and fit to extract the association constants, K_a, as described elsewhere [23]. Reported errors originate from the global fit of two to three collected data sets. Both, 1 NMM:1 DNA and 1 NMM:2 DNA binding models were considered. Changes in fluorescence intensity at λ_{max} (610 nm for NMM and 607-609 nm for

NMM bound to DNA) are reported as fluorescence enhancement and were calculated by taking the difference between the fluorescence intensity in the presence and absence of DNA divided by the fluorescence intensity recorded for NMM alone. Uncertainties in the fluorescence intensities arise predominantly from lamp intensity variation at the excitation wavelength from day to day and errors associated with pipetting small volumes. Error bars on fluorescence enhancement values are one standard deviation (confidence interval of 68.2%), derived from replicate experiments. Statistical analysis performed on the fluorescence enhancement data can be found in SI, Tables S3 and S4.

Competition titrations via fluorescence. To determine NMM's selectivity for GQ structures, two sets of competition titrations were performed. In one set, a solution of 1.0 μmol L^{-1} NMM containing approximately 10 μmol L^{-1} of G4 or VEGF was titrated with increasing amounts of dsDNA. In another set of experiments, a solution of 1.0 μmol L^{-1} NMM containing up to 100 μmol L^{-1} of dsDNA was titrated with an increasing amount of G4 or VEGF. These titrations were performed at 25 °C in TB (G4) or 5K (VEGF) buffers.

pH studies. To measure the effect of pH on NMM fluorescence, 1 μmol L^{-1} to 2 μmol L^{-1} NMM in H$_2$O was titrated with 0.1 mol L^{-1} of either HCl or NaOH to achieve the desired pH. The pH, fluorescence, and UV-vis data were collected after each addition of acid or base. The experiments were run either as titrations or using a batch method. For fluorescence, slits were 3.5 nm to 5 nm. Titrations were repeated four times.

The reversibility of the NMM signal change as a function of pH was tested in the following way. UV-vis and fluorescence spectra of two NMM samples were recorded at neutral pH. The pH of the first sample was brought down to about 3.2, then back up to neutral pH. The pH of the second sample was brought up to about 10.5, then back down to neutral pH. The solution pH was adjusted using either 0.25 mol L^{-1} HCl or 0.25 mol L^{-1} LiOH. These experiments were repeated twice.

Finally, the effect of pH and buffer type on NMM's fluorescence was tested in five buffers that span the pH range from 4.0 to 8.3. These buffers contained 10 mmol L^{-1} of Tris (pH = 8.3), lithium cacodylate (pH = 7.2 and 5.8), or sodium acetate (pH = 4.9 and 4.0). All buffers were supplemented with 5 mmol L^{-1} KCl and 95 mmol L^{-1} LiCl.

Fluorescence lifetime measurements. Fluorescence lifetimes were collected for NMM in the presence of representative GQ structures on a multi-frequency cross-correlation phase and modulation frequency fluorometer at room temperature [35, 36]. Samples were prepared at concentrations of NMM ranging from 0.7 μmol L^{-1} to 2.3 μmol L^{-1} with GQ ratios ranging from 1:4 to 1:30, depending on the sequence. The excitation wavelength was 399 nm; sample emission was filtered through a 550 nm longpass filter and referenced to a scatterer with counts that were matched to that of the sample. The frequency range over which data were collected was 1 MHz to 250 MHz. The number of frequencies collected varied from 10 to 50, depending on the sample. Lifetimes were calculated from fits to the phase delay and modulation ratio data as described in the literature using commercially available software [37]. Errors are either associated with global fits to multiple scans or are one standard deviation calculated from multiple lifetime measurements for a given sample. The low fluorescence intensity of free NMM in a buffer made it impossible to measure its lifetime accurately with our instrumentation.

RESULTS AND DISCUSSION

In light of the exceptional selectivity of NMM for G-quadruplex DNA relative to other DNA secondary structures [24, 25] and this ligand's unique ability to discriminate between parallel vs. antiparallel GQ conformation [23], we set out to determine if NMM could be used as GQ-specific fluorescence probe. To achieve this goal, we measured the fluorescence of NMM in the presence of a variety of DNA sequences and secondary structures, including ssDNA, dsDNA, i-motif DNA as well as carefully selected GQ DNA with representative folding topologies (Table 1). GQ secondary structures are usually defined as follows. Mixed-hybrid quadruplexes contain one strand running in the opposite direction from the other three strands, as shown in Fig. 1B, left. Antiparallel GQs contain two strands that run in opposite direction from the two remaining strands, for example, the bimolecular GQ shown in Fig. 1B, middle. A parallel-stranded GQ has all four DNA strands running in the same direction as shown in Fig. 1B, right, for a tetramolecular GQ. The secondary structure of each DNA in this study was verified using CD spectroscopy, Fig. S1 and S2.

Quadruplex sequences chosen in this work include oncogene promoters, telomeric DNA and some synthetic sequences. Specifically, Tel22 [38] and 26TelG4 are human telomeric DNA sequences; $G_4T_4G_4$ is telomeric DNA from the ciliate *Oxytricha nova*. This latter sequence was chosen because it maintains antiparallel topology both in potassium [39] and in sodium buffers [40]. G4TERT corresponds to a DNA sequences in the promoter of hTERT, a catalytic domain of telomerase [41]. Oncogene promoters tested in this work include VEGF, Blc-2, cKit, and cMyc. VEGF is a promoter gene for vascular endothelial growth factor that is upregulated in a variety of cancers [14]; Bcl-2 inhibits cell apoptosis in B-cell lymphoma cancer cell lines [42]; cKit is a tyrosine kinase receptor that controls cell growth [43]; and cMyc is a transcriptional regulator of ~15% of human genes involved in a variety of cancers [44]. In addition, we tested non-physiological DNA sequences that are models for GQs. The thrombin binding aptamer, TBA [45], was used in this work because, like $G_4T_4G_4$, it forms an antiparallel topology regardless of buffer condition; G4 and G8 always form simple homogeneous tetramolecular parallel quadruplexes; and IL1 forms a parallel-stranded quadruplex with single-stranded overhangs that contain nucleotides other than thymine.

9

Titration of NMM with parallel and antiparallel GQs monitored by fluorescence to determine saturation limit and binding constants. NMM fluoresces weakly in aqueous solution, but its fluorescence increases dramatically in the presence of certain DNA structures [26]. Thus NMM can serve as a "turn-on" fluorescent probe. To determine the amount of DNA required to reach NMM's fluorescence signal saturation point, we performed fluorescence titrations of NMM using a subset of DNA sequences. Titration data for the tetramolecular parallel quadruplexes, G4 and G8, and for the antiparallel/mixed-hybrid quadruplex $G_4T_4G_4$ are shown in Fig. 2; data for the intramolecular parallel quadruplex, VEGF, are shown in the SI Fig. S3. These data indicate that at least 5 equivalents of GQ DNA are required to saturate NMM fluorescence. For consistency, in all subsequent experiments 10 equivalents of DNA structural element were used per NMM molecule.

Our titration data allowed determination of binding constants. The fluorescence intensity at 609 nm as a function of added GQ DNA was fit to a 1:1 binding model, yielding K_a of $(1.4 \pm 0.2) \times 10^6$ L mol^{-1} for G4, $(1.7 \pm 0.2) \times 10^6$ L mol^{-1} for G8, and $(1.1 \pm 0.1) \times 10^6$ L mol^{-1} for VEGF. Fits improved (as judged by residuals) for VEGF when NMM to GQ binding ratio was changed to 1:2, yielding K_a of $(7.0 \pm 0.9) \times 10^6$ L mol^{-1}. We utilized Job plot experiments (method of continuous variation) to verify independently the stoichiometry of NMM-VEGF interaction. Analysis of the Job plot indicates either a 1:1 or 1:2 binding stoichiometry (Fig. S3B). From these data we conclude that one molecule of NMM binds two molecules of VEGF when VEGF is in excess, but binds only one molecule of VEGF when concentrations of DNA and NMM are comparable.

$G_4T_4G_4$ quadruplex, which adopts an antiparallel/mixed-hybrid topology in potassium buffer, displayed tight binding to NMM with K_a of $(1.26 \pm 0.07) \times 10^7$ L mol^{-1} using a 1:1 binding model. This affinity is two orders of magnitude higher than the previously reported binding affinity of NMM to a different mixed-hybrid quadruplex, Tel22, 1.0×10^5 L mol^{-1} [23]. Overall, NMM's affinity for the GQ structures decreases in the following order: $G_4T_4G_4$ > VEGF ≈ G8 ≈ G4 > Tel22. This ordering correlates qualitatively with higher steady-state NMM fluorescence in the presence of $G_4T_4G_4$, G4, G8 and VEGF as compared to Tel22 (below, Fig. 3). The tight binding between NMM and $G_4T_4G_4$ is somewhat puzzling. In potassium buffer $G_4T_4G_4$ forms an antiparallel dimer [39], which would leave no room for NMM binding. Currently, our lab is

investigating the details of this interaction to uncover possible reasons for this seemingly anomalous behavior.

When NMM was titrated with predominantly antiparallel $G_4T_4G_4$ and 26TelG4, both in 50Na buffer, the fluorescence intensity increased in a linear fashion with increasing DNA concentration (Fig. S4), not reaching saturation even at > 16-fold excess of DNA over NMM. The observed fluorescence increase is well below that obtained for $G_4T_4G_4$ in 5K buffer. This observed linear dependence suggests weak and/or nonspecific binding of NMM to these sequences.

The presence of parallel GQs increases NMM steady-state fluorescence intensity and fluorescence lifetime. To establish NMM's utility as a fluorescent probe for quadruplex detection, we determined how NMM's fluorescence changes in the presence of a 10-fold excess of a variety of DNA structures. Fig. 3 illustrates that ssDNA and dsDNA have little effect on NMM fluorescence in agreement with previous equilibrium dialysis experiments [24]. These same equilibrium dialysis experiments indicated significant binding between NMM and the i-motifs TC_4T, and $C_4T_4C_4$ [24]. In contract, we did not observe fluorescence increases in the presence of any of the i-motifs we tested (i-cMyc, C8, TC_4T, and $C_4T_4C_4$). This discrepancy could be due to the difference in experimental conditions and nature of techniques utilized to observe interaction between NMM and DNA. Specifically, the buffer used in the equilibrium dialysis experiments contained 6 mmol L^{-1} Na_2HPO_4, 2 mmol L^{-1} NaH_2PO_4, 1 mmol L^{-1} Na_2EDTA, and 185 mmol L^{-1} NaCl, pH 7.0, while our buffer, 5K 5.8, had lower ionic strength, lower pH and 5 mmol L^{-1} KCl. NMM's insensitivity to i-motifs (at least as reported by fluorescence and UV-vis) emphasizes further its exceptional selectivity for GQ DNA structures.

NMM's steady-state fluorescence increases in the presence of GQ DNA. We investigated the specificity of this increase by utilizing selected G-rich oligonucleotides that adopt well-defined secondary structures including parallel, mixed-hybrid, and antiparallel, Table 1. IL1, G4, G8, cMyc, cKit2, and VEGF sequences adopt parallel-stranded topology alone or in the presence of NMM on the basis of our CD spectra ([23] and Fig. S1). Addition of a 10-fold excess of these DNA structures to NMM lead to fluorescence enhancement of more than 50 (Fig. 3, Table 1) with the only exception being cKit2, for which the fluorescence enhancement is

46. Sequences exhibiting starting parallel/mixed-hybrid conformations, such as cKit1, G4TERT, and Bcl-2 generally lead to fluorescence enhancement of 42 to 50.

Sequences with predominantly mixed-hybrid GQ topology, such as Tel22 and 26TelG4 in 5K buffer [23], lead to significantly smaller fluorescence enhancement of 25 and 34, respectively. As in the titration experiments, $G_4T_4G_4$ GQ in 5K buffer produces an anomalous result. This sequence adopts an antiparallel/mixed-hybrid topology (CD data, Fig. S2), yet leads to fluorescence enhancement of 60, similar to that caused by parallel GQ structures. A large increase in NMM's fluorescence upon addition of $G_4T_4G_4$ in 10 mmol L^{-1} HEPES buffer with 150 mmol L^{-1} NaCl and 5 mmol L^{-1} KCl was also reported earlier [25]. A possible explanation is that NMM might convert $G_4T_4G_4$ to a structure (or a mixture) containing significant parallel component. Indeed, increased parallel component is detected by CD for this sequence under conditions of 2-fold NMM excess (Fig. S2). It is important to keep in mind that the fluorescence samples contained 10-fold excess DNA, not excess NMM, leading us to expect that only a small fraction of GQ DNA could be structurally altered by NMM if it acts in a stoichiometric fashion.

Incubating NMM with predominantly antiparallel G-rich sequences resulted in only a small fluorescence increase, the lowest of which was observed for Tel22 and TBA in 50Na, 1.6 and 5.2, respectively. Low fluorescence enhancements suggest a lack of interaction between NMM and these antiparallel structures, consistent with our earlier report [23]. This interpretation is further supported by CD annealing studies in which NMM failed to induce changes in these DNA structures ([23] and Fig. S2). Other sequences in this group, $G_4T_4G_4$ and 26TelG4 in 50Na or TBA in 5K caused small, but significant, increases in NMM fluorescence. These increases, however, are three to six times lower than those observed for parallel GQ sequences. We tested whether NMM has an effect on the folds of these sequences by CD annealing ([23] and Fig. S2) and observed that the topologies of 26TelG4 in 50Na and TBA in 5K do not change in the presence of NMM. In contrast, addition of NMM to $G_4T_4G_4$ in 50Na leads to an increase in CD signal at 264 nm, consistent with an increase in parallel component of GQ structure. Our result differs from a previous report indicating that annealing of $G_4T_4G_4$ DNA with 1 equivalent of NMM in a buffer containing 140 mmol L^{-1} NaCl does not change its CD signal [46]. This discrepancy is most likely due to the lower amount of NMM used in the latter study and, possibly, to differences in buffer composition.

12

The presence of high concentration of potassium ions shifts folding equilibria toward fully-folded GQ structures with higher parallel component. Potassium is also known to significantly stablizise GQ conformations minizing ligands ability to affect quadruplex topology. To test this possibility we performed fluorescence experiments in 150K buffer, Figure S5A. Under this condition, most of the DNA sequences (cKit1, cKit2, G4TERT, and Bcl-2, 26TelG4, and $G_4T_4G_4$) displayed a significant increase in CD spectral intensity at 264 nm, Fig. S5B. Overall, fluorescence increase data resemble those collected in 5K buffer. Notably, all of the parallel (or predominantly parallel) sequences (G4, G4TERT, Bcl-2, Kit2, cMyc, VEGF) generate somewhat lower enhancement of NMM fluorescence in 150K vs. 5K buffer; the only exception is cKit1, which exhibits an unchanged fluorescence. The small decrease in fluorescence enhancement observed in 150K buffer could be explained by weaker binding of NMM to DNA at this increased ionic strength. In contrast, NMM in the presence of mixed-hybrid (Tel22), antiparallel (TBA), or predominantly antiparallel (26TelG4) quadruplexes showed an increase in fluorescence enhancement in 150K vs. 5K buffer, as would be expected for quadruplexes with increased parallel component. $G_4T_4G_4$ GQ once again displayed anomalous behavior characteristic of parallel GQs and not mixed-hybrid GQs. It is important to emphasize that the overall trends of fluorescence enhancement were reproducible in buffers with low and high potassium ion concentrations.

Statistical analysis of the fluorescence enhancement data confirms NMM's unique selectivity toward GQs vs. non-quadruplex structures (Table S4). For example, the fluorescence of NMM at 610 nm is on average 150- and 390-times higher in the presence of Tel22 and G8 (in 5K) vs. dsDNA, respectively. More importantly, NMM can differentiate GQ structures based on their strand orientation. The fluorescence enhancement values increase in the following order, antiparallel < mixed-hybrind < parallel. The ratio of fluorescence enhancements for predominantly parallel GQs (inter- or intramolecular) vs. antiparallel GQ is 5.9 and vs. mixed-hybrid is 2.0 when the values in each category are averaged (Table S3). In previous equilibrium dialysis experiments, discrimination ratio of 2 was reported [24]. This ratio appears to depend on the identity of the G-rich sequences and on buffer conditions.

When different conformations of Tel22 are compared (mixed-hybrid in K^+-buffer, antiparallel in Na^+-buffer and predominantly single-stranded in Li^+-buffer), NMM's preference for mixed-hybrid (or possibly parallel fold) is obvious (Fig. S6). The overall discrimination

pattern for NMM is similar to that of another recently reported fluorescent probe, APD [21]. However, the fluorescence of APD did not increase in the presence of Tel22, contrary to our observation with NMM; the effect of i-motifs on APD was not reported.

We hypothesized that the observed increase in steady-state emission of NMM in the presence of GQs is a result of protection of NMM from dynamic quenching by water. To test this idea, we performed two experiments. First, fluorescence lifetimes were collected for NMM in the presence of representative quadruplex topologies; data are summarized in Table 1. The fluorescence lifetime of NMM is the longest (6 ns to 8 ns) in the presence of predominantly parallel-stranded GQs. In contrast, NMM exhibits two lifetimes (5 ns to 7 ns and 1 ns to 2 ns) when it interacts with antiparallel or mixed-hybrid GQ structures. The key result is that the steady-state fluorescence enhancements roughly correlate with fluorescence lifetimes (Fig. S7A). In the second experiment, we used isotopic substitution of deuterium oxide (D_2O) for water because D_2O decreases dynamic quenching of fluorophores [47]. As predicted, NMM's steady-state fluorescence intensity in D_2O increased relative to that in H_2O (Fig. S7B). Results of both experiments are consistent with our hypothesis that binding of NMM to a quadruplex protects it from solvent leading to increased fluorescence.

NMM fluorescence detects parallel-stranded GQ's in the presence of duplex DNA. It is important that quadruplex DNA should be recognized by its probe even in the context of a large background of dsDNA. To demonstrate that NMM is capable of such selective recognition, we performed two sets of competition experiments. A solution of NMM containing > 10 fold-excess of the parallel-stranded G4 or VEGF quadruplex was titrated with increasing amounts of C1A:C1B dsDNA or genomic CT dsDNA, respectively. In both cases, NMM's fluorescence did not change even when a 100-fold excess of dsDNA was added, Fig. S8. This is consistent with previous experiments, where we observed that the melting temperature of NMM-stabilized Tel22 did not decrease even in the presence of 480-fold excess dsDNA [23]. In a reverse competition experiment, a solution of NMM with 100-fold excess duplex was titrated with increasing amounts of either G4 or VEGF quadruplex. In both cases, the titration data were practically indistinguishable from the titrations of NMM (alone, in the absence of duplex) with GQ (Fig. S3C for VEGF case). The binding constants obtained for NMM-VEGF complex with or without

14

CT DNA are within experimental error of each other, $(6.9 \pm 1.5) \times 10^6$ L mol^{-1} and $(7.0 \pm 0.9) \times 10^6$ L mol^{-1}, respectively (assuming 2:1 GQ:NMM binding stoichiometry).

Disruption of GQ structure decreases NMM fluorescence. Treatment of GQ structures with LiOH dissociates DNA strands. This process is driven by deprotonation of the N1 site on guanine at a pH above its pK_a of 9.4, which leads to electrostatic repulsion of the strands. We observed unfolding of G4 or IL1 GQs upon their treatment with LiOH via CD spectroscopy (see Fig. S1 for IL1). When NMM was incubated with G4 or IL1, its fluorescence increased as expected, but fell to levels typical for NMM alone upon subsequent treatment with LiOH, Fig. S9. These results further highlight the ability of NMM to discriminate between GQ DNA and other DNA structures (single-stranded in this case).

NMM fluorescence is predominantly independent of pH and buffer composition.
Physiological pH varies from 7 to 9, thus it is ideal that the potential fluorescent probe remains insensitive to changes in pH in this range. To test NMM's sensitivity to pH, an aqueous solution of NMM was titrated either with acid, HCl, or base, NaOH. The NMM fluorescence spectrum retained its overall shape, but slightly increased in intensity (by 1.5 to 2.0 times) when the pH was increased from 2.0 to 8.6 (Fig. S10A). Upon further pH increase, a new signal emerged at 636 nm that was at least 25 times more intense than the signal in the original spectrum (Fig. S10B). Observed pH changes were reversible, as addition of acid to a basic solution of NMM regenerated the starting NMM fluorescence spectrum (Fig. S10C). Neutralization of the acidic solution of NMM lead to a relatively small change in spectral shape and intensity (Fig. S10D).

Because working with biological molecules requires buffered solutions, we tested NMM's fluorescence in five commonly used buffers over a wide pH range: 8.3 (Tris), 7.2 and 5.8 (lithium cacodylate), 4.9 and 4.0 (sodium acetate). Again, NMM displayed only a small (about 1.3 times) decrease in fluorescence intensity with decreasing pH, Fig. S11.

We proceeded to test NMM's fluorescence in the presence of selected DNA sequences in two potassium-containing buffers, lithium cacodylate at pH 7.2 (5K) and in Tris at pH 8.3 (TB). Direct comparison of the increase in NMM fluorescence induced by G4 and G8 reveals that the values in TB are slightly lower than in 5K: 65 ± 11 vs. 68 ± 4 for G4 and 58 ± 4 vs. 70 ± 4 for G8. Both measurements show, however, that NMM fluorescence increases significantly and

reproducibly in the presence of parallel quadruplex, indicating that the enhancement is observed easily over a range of experimental conditions.

In short, NMM's fluorescence is only weakly sensitive to the nature of the buffer or the pH (in the physiological pH range) making it highly suitable for biologic detection of quadruplex DNA. It is important to keep in mind that the amount and type of monovalent cation as well as solution pH can modulate DNA structure and, therefore, DNA interactions with NMM effecting NMM's fluorescence.

CONCLUSION

For use in fluorescence microscopy, a candidate dye should possess a large extinction coefficient, be selective toward its target and have an acceptable quantum yield. NMM meets the first criterion: its extinction coefficient is 1.45×10^5 M^{-1} cm^{-1} [28] and it shows an approximately 20 nm red shift of its Soret band upon DNA binding [23]. Duplex-binding dyes, like propidium iodide, that are used routinely for fluorescence microscopy of DNA, exhibit a 20 to 30 fold increase in fluorescence when bound to DNA. NMM displays little change in fluorescence intensity in the presence of ssDNA (regardless of G-content), dsDNA, or i-motif DNA, and a modest increase in fluorescence in the presence of antiparallel quadruplexes. In striking contrast, NMM's fluorescence increases more than 40 times upon addition of parallel-stranded GQ DNA, making it an attractive "light-switch" fluorescent probe. The sequence Tel22, which is a fragment of the human telomeric repeat, leads to a 28 ± 2 fold enhancement in NMM's fluorescence in 5K buffer (where Tel22 exist in a mixed-hybrid form) but only a 2.6 ± 0.2 fold enhancement in 50Na buffer (where it adopts antiparallel topology) or 2.2 ± 0.2 fold enhancement in 100Li buffer (where Tel22 is single-stranded), indicating that discrimination of the type of fold adopted by the human telomeric sequence *in vivo* could be achieved with fluorescence microscopy of NMM-stained samples.

ACKNOWLEDGMENTS

SUPPLEMENTARY DATA are available online: Supplementary tables S1 – S4, Supplementary figures 1-11, and Supplementary methods.

REFERENCES

1. Williamson, J. R., Raghuraman, M. K. & Cech, T. R. (1989) Monovalent cation-induced structure of telomeric DNA: the G-quartet model, *Cell.* **59**, 871-880.
2. Sen, D. & Gilbert, W. (1992) Guanine quartet structures, *Methods Enzymol.* **211**, 191-9.
3. Kang, C., Zhang, X., Ratliff, R., Moyzis, R. & Rich, A. (1992) Crystal structure of four-stranded Oxytricha telomeric DNA, *Nature.* **356**, 126-131.
4. Sen, D. & Gilbert, W. (1990) A sodium-potassium switch in the formation of four-stranded G4-DNA, *Nature.* **344**, 410-414.
5. Burge, S., Parkinson, G. N., Hazel, P., Todd, A. K. & Neidle, S. (2006) Quadruplex DNA: sequence, topology, and structure, *Nucleic Acids Res.* **34**, 5402-5415.
6. Esposito, V., Galeone, A., Mayol, L., Oliviero, G., Virgilio, A. & Randazzo, L. (2007) A topological classification of G-quadruplex structures., *Nucleosides Nucleotides Nucleic Acids.* **26**, 1155-9.
7. Li, J., Correia, J. J., Wang, L., Trent, J. O. & Chaires, J. B. (2005) Not so crystal clear: the structure of the human telomere G-quadruplex in solution differs from that present in a crystal, *Nucleic Acids Res.* **33**, 4649-59.
8. Haider, S. M., Parkinson, G. N. & Neidle, S. (2003) Structure of a G-quadruplex-ligand complex, *J Mol Biol.* **326**, 117-125.
9. Parkinson, G. N., Lee, M. P. H. & Neidle, S. (2002) Crystal structure of parallel quadruplexes from human telomeric DNA, *Nature.* **417**, 876-880.
10. Huppert, J. L. & Balasubramanian, S. (2007) G-quadruplexes in promoters throughout the human genome, *Nucleic Acids Res.* **35**, 406-13.
11. Di Antonio, M., Rodriguez, R. & Balasubramanian, S. (2012) Experimental approaches to identify cellular G-quadruplex structures and functions, *Methods.* **57**, 84-92.
12. Bugaut, A. & Balasubramanian, S. (2012) 5'-UTR RNA G-quadruplexes: translation regulation and targeting, *Nucleic Acids Res.* **40**, 4727–4741.
13. Todd, A. K. & Neidle, S. (2011) Mapping the sequences of potential guanine quadruplex motifs, *Nucleic Acids Res.* **39**, 4917-4927.
14. Sun, D. K., Guo, K. X. & Shin, Y. J. (2011) Evidence of the formation of G-quadruplex structures in the promoter region of the human vascular endothelial growth factor gene, *Nucleic Acids Res.* **39**, 1256-1265.
15. Mathad, R. I., Hatzakis, E., Dai, J. X. & Yang, D. Z. (2011) c-MYC promoter G-quadruplex formed at the 5 '-end of NHE III1 element: insights into biological relevance and parallel-stranded G-quadruplex stability, *Nucleic Acids Res.* **39**, 9023-9033.
16. Bochman, M. L., Paeschke, K. & Zakian, V. A. (2012) DNA secondary structures: stability and function of G-quadruplex structures, *Nat Rev Genet.* **13**, 770-780.
17. Vummidi, B. R., Alzeer, J. & Luedtke, N. W. (2013) Fluorescent probes for G-quadruplex structures, *ChemBioChem.* **14**, 540-558.
18. Biffi, G., Tannahill, D. & Balasubramanian, S. (2012) An intramolecular G-quadruplex structure is required for binding of telomeric repeat-containing RNA to the telomeric protein TRF2, *J Am Chem Soc.* **134**, 11974-11976.
19. Monchaud, D. & Teulade-Fichou, M.-P. (2008) A hitchhiker's guide to G-quadruplex ligands, *Org Biomol Chem.* **6**, 627-636.
20. Georgiades, S. N., Karim, N. H. A., Suntharalingam, K. & Vilar, R. (2010) Interaction of metal complexes with G-quadruplex DNA, *Angew Chem Int Ed.* **49**, 4020-4034.

21. Nikan, M., Di Antonio, M., Abecassis, K., McLuckie, K. & Balasubramanian, S. (2013) An acetylene-bridged 6,8-purine dimer as a fluorescent switch-on probe for parallel G-quadruplexes, *Angew Chem Int Ed.* **52**, 1428-1431.

22. Biffi, G., Tannahill, D., McCafferty, J. & Balasubramanian, S. (2013) Quantitative visualization of DNA G-quadruplex structures in human cells, *Nat Chem.* **5**, 182-186.

23. Nicoludis, J. M., Barrett, S. P., Mergny, J.-L. & Yatsunyk, L. A. (2012) Interaction of human telomeric DNA with N-methyl mesoporphyrin IX, *Nucleic Acids Res.* **40**, 5432-5447.

24. Ragazzon, P. & Chaires, J. B. (2007) Use of competition dialysis in the discovery of G-quadruplex selective ligands, *Methods.* **43**, 313-323.

25. Arthanari, H., Basu, S., Kawano, T. L. & Bolton, P. H. (1998) Fluorescent dyes specific for quadruplex DNA, *Nucleic Acids Res* **26**, 3724-3728.

26. Paramasivan, S. & Bolton, P. H. (2008) Mix and measure fluorescence screening for selective quadruplex binders, *Nucleic Acids Res.* **36**, e106.

27. Nicoludis, J. M., Miller, S. T., Jeffrey, P. D., Barrett, S. P., Rablen, P. R., Lawton, T. J. & Yatsunyk, L. A. (2012) Optimized end-stacking provides specificity of N-methyl mesoporphyrin IX for human telomeric G-quadruplex DNA, *J Am Chem Soc* **134**, 20446-20456.

28. Ren, J. & Chaires, J. B. (1999) Sequence and Structural Selectivity of Nucleic Acid Binding Ligands, *Biochemistry.* **38**, 16067-16075.

29. Fahlman, R. P. & Sen, D. (1999) "Synapsable" DNA Double Helices: Self-Selective Modules for Assembling DNA Superstructures, *J Am Chem Soc.* **121**, 11079-11085.

30. Leroy, J.-L., Guéron, M., Mergny, J.-L. & Hélène, C. (1994) Intramolecular folding of a fragment of the cytosine-rich strand of telomeric DNA into an i-motif, *Nucleic Acids Res.* **22**, 1600-1606.

31. Sambrook, J. & Russell, D. (2001) *Molecular Cloning A Laboratory Manual*, 3rd edn, Cold Spring Harbor Laboratory Press, Cold Spring Harbor.

32. Borer, P. N. (1975) Optical Properties of Nucleic Acids, Absorption, and Circular Dichroism Spectra in *Handbook of Biochemistry and Molecular Biology* (Fasman, G., ed) pp. 589, CRC Press, Cleveland.

33. Tataurov, A. V., You, Y. & Owczarzy, R. (2008) Predicting ultraviolet spectrum of single stranded and double stranded deoxyribonucleic acids, *Biophys Chem.* **133**, 66-70.

34. Bhattacharjee, A. J., Ahluwalia, K., Taylor, S., Jin, O., Nicoludis, J. M., Buscaglia, R., Brad Chaires, J., Kornfilt, D. J. P., Marquardt, D. G. S. & Yatsunyk, L. A. (2011) Induction of G-quadruplex DNA structure by Zn(II) 5,10,15,20-tetrakis(N-methyl-4-pyridyl)porphyrin, *Biochimie.* **93**, 1297-1309.

35. Gratton, E., Alcala, J. R. & Barbieri, B. (1991) Frequency domain fluorometry in *Handbook of Luminescence Techniques in Chemical and Biochemical Analysis*, Marcel Dekker, Inc., , New York, NY, USA.

36. Lackowicz, J. R. (2006) *Principles of Fluorescence Spectroscopy*, 3d edn, Springer Science+Business Media, LLC, 233 Spring Street, New York, NY 10013, USA.

37. Jameson, D. M. & Gratton, E. (1983) Analysis of Heterogeneous Emissions by Multifrequency Phase and Modulation Fluorometry in *New Directions in Molecular Luminescence* (Eastwood, D., ed) pp. 67-81, ASTM STP 822, American Society of Testing and Materials, Philadelphia, PA, USA.

38. Phan, A. T. (2010) Human telomeric G-quadruplex: structures of DNA and RNA sequences, *FEBS J.* **277**, 1107-1117.

39. Haider, S., Parkinson, G. N. & Neidle, S. (2002) Crystal Structure of the Potassium Form of an *Oxytricha nova* G-quadruplex, *J Mol Biol.* **320**, 189-200.

40. Schultze, P., Smith, F. W. & Feigon, J. (1994) Refined solution structure of the dimeric quadruplex formed from the Oxytricha telomeric oligonucleotide d(GGGGTTTTGGGG), *Structure.* **2**, 221-233.

41. Lim, K. W., Lacroix, L., Yue, D. J. E., Lim, J. K. C., Lim, J. M. W. & Phan, A. T. (2010) Coexistence of two distinct G-quadruplex conformations in the hTERT promoter, *J Am Chem Soc.* **132**, 12331-12342.

42. Dai, J., Dexheimer, T. S., Chen, D., Carver, M., Ambrus, A., Jones, R. A. & Yang, D. (2006) An intramolecular G-quadruplex structure with mixed parallel/antiparallel G-strands formed in the human BCL-2 promoter region in solution, *J Am Chem Soc.* **128**, 1096-1098.

43. Phan, A. T., Kuryavyi, V., Burge, S., Neidle, S. & Patel, D. J. (2007) Structure of an unprecedented G-quadruplex scaffold in the human c-kit promoter, *J Am Chem Soc.* **129**, 4386-4392.

44. Gonzalez, V. & Hurley, L. H. (2010) The c-MYC NHE III1: function and regulation, *Annu Rev Pharmacol Toxicol.* **50**, 111-129.

45. Macaya, R. F., Schultze, P., Smith, F. W., Roe, J. A. & Feigon, J. (1993) Thrombin-binding DNA aptamer forms a unimolecular quadruplex structure in solution, *Proc Natl Acad Sci.* **90**, 3745-3749.

46. Paramasivan, S., Rujan, I. & Bolton, P. H. (2007) Circular dichroism of quadruplex DNAs: Applications to structure, cation effects and ligand binding, *Methods.* **43**, 324-331.

47. Förster, T. & Rokos, K. (1967) A deuterium isotope solvent effect on fluorescence, *Chem Phys Lett.* **1**, 279-280.

Table 1: Oligonucleotide Conformation and Fluorescence Enhancement and Lifetime data

| Name | Conformation[a] | | Fluorescence enhancement | Fluorescence lifetimes[b] (τ_1, ns) |
	Without NMM	With NMM		
C1A	ss	ss	0.69 ± 0.19 (TB)	
Tel22, 100Li	ss	ss	1.22 ± 0.21 (100Li)	
CT	ds	ds	0.00 ± 0.05 0.03 ± 0.07 (50Na)	
ds26	ds	ds	0.25 ± 0.06	
C1A:C1B	ds	ds	0.44 ± 0.22 (TB)	
C8	i	i	1.25 ± 0.65 (5K 5.8)	
i-cMyc	i	i	1.53 ± 0.12 (5K 5.8)	
$C_4T_4C_4$	i	i	0.45 ± 0.16 (5K 5.8)	
TC_4T	i	i	0.44 ± 0.00 (5K 5.8)	
IL1	P	P	55.7 ± 6.8 (TB)	
G4	P	P	67.8 ± 4.3 65 ± 11 (TB)	7.83 ± 0.01 8.29 ± 0.01 (TB)
G8	P	P	69.9 ± 3.7 57.5 ± 4.2 (TB)	8.00 ± 0.01 7.97 ± 0.01 (TB)
VEGF	P	P	52.9 ± 2.0	7.09 ± 0.01
cMyc	P	P	64.8 ± 3.8	7.96 ± 0.01
cKit2	P	P	46.3 ± 1.6	6.35 ± 0.01
cKit1	P/M	P	41.9 ± 2.5	
G4TERT	P/M	P	50.2 ± 6.1	
Bcl-2	P/M	P	47.9 ± 1.2	
Tel22	M	P	25.5 ± 2.4	$\tau_1 = 7.26 ± 0.02$ (89) $\tau_2 = 2.00 ± 0.03$ (11)
26TelG4	A/M	M	34.1 ± 4.6	

$G_4T_4G_4$	A/M	M	60.2 ± 4.6	7.13 ± 0.01
Tel22, 50Na	A	A	1.59 ± 0.18	$\tau_1 = 5.18 \pm 0.01 \ (60 \pm 2)$ $\tau_2 = 0.68 \pm 0.002 \ (40 \pm 2)$
TBA, 5K	A	A	15.5 ± 1.4	$\tau_1 = 5.81 \pm 0.01 \ (90 \pm 4)$ $\tau_2 = 1.07 \pm 0.01 \ (10 \pm 4)$
TBA, 50Na	A	A	5.15 ± 0.39	
26TelG4, 50Na	A	A	12.1 ± 1.3	
$G_4T_4G_4$, 50Na	A	A/M	16.0 ± 1.1	$\tau_1 = 6.85 \pm 0.002 \ (88 \pm 3)$ $\tau_2 = 1.34 \pm 0.01 \ (12 \pm 3)$

[a] ss = single-stranded; P = parallel; A = antiparallel; ds = double-stranded (duplex); M = mixed; i = i-motif; buffer is 5K unless specified otherwise;

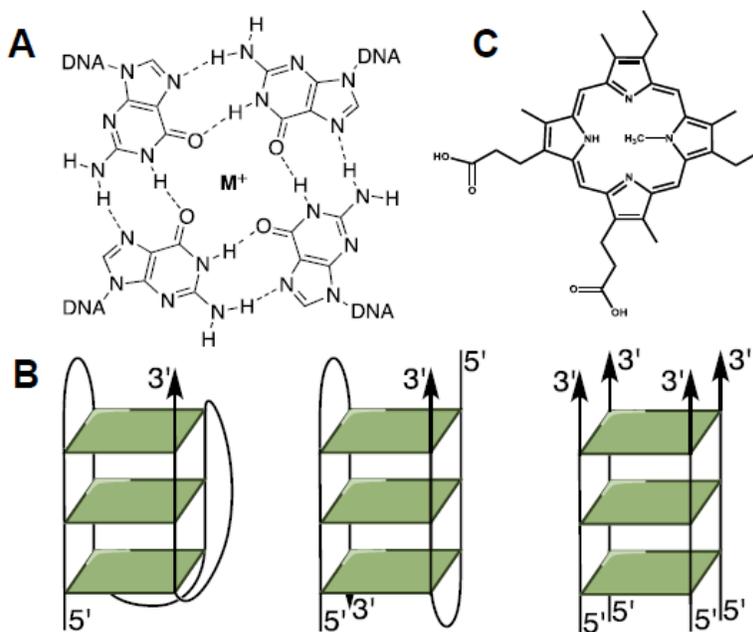[b] population is given in parenthesis as % and is 100% if not specified.

Fig. 1. Structures of GQ and NMM. (**A**) Structure of a G-tetrad. (**B**) Schematic representations of mixed-hybrid monomolecular GQ (left), antiparallel bimolecular GQ (middle) and tetramolecular parallel-stranded GQ (right). (**C**) Structure of NMM. Note that commercially available NMM is a mixture of four regioisomers that differ in the position of the N-Me group (only one isomer is shown); each forms a pair of enantiomers with the N-Me group pointing up or down.
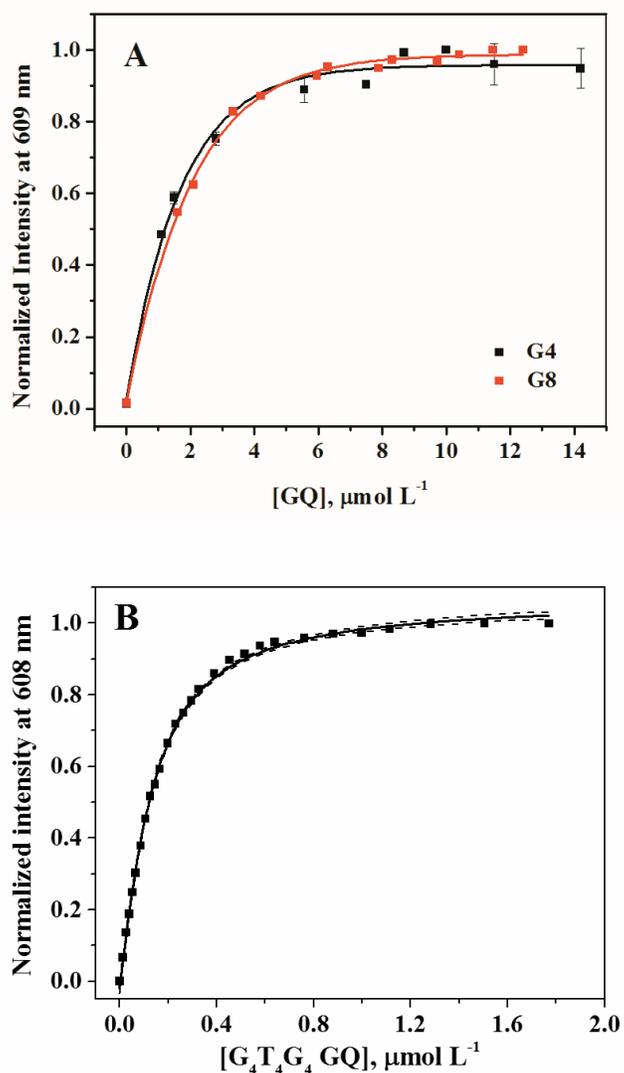
Fig. 2. Normalized fluorescence data for titration of A) 1.0 µmol L^{-1} NMM with G4 and G8 in TB buffer, and B) 0.1 µmol L^{-1} NMM with $G_4T_4G_4$ in 5K buffer at 25 °C. Data for G4 and G8 are average of three individual titrations. Solid lines represent global fits to a 1:1 binding model and dashed lines represent the 95 % confidence interval. Binding constants were determined to be $(1.4 \pm 0.2) \times 10^6$, $(1.7 \pm 0.2) \times 10^6$, and $(1.26 \pm 0.07) \times 10^7$ L mol^{-1} for G4, G8, and $G_4T_4G_4$, respectively. Note, the data for $G_4T_4G_4$ could be satisfactory fit to a 1 NMM:2 GQ binding model with K_a of $(5.4 \pm 0.5) \times 10^7$ L mol^{-1}.
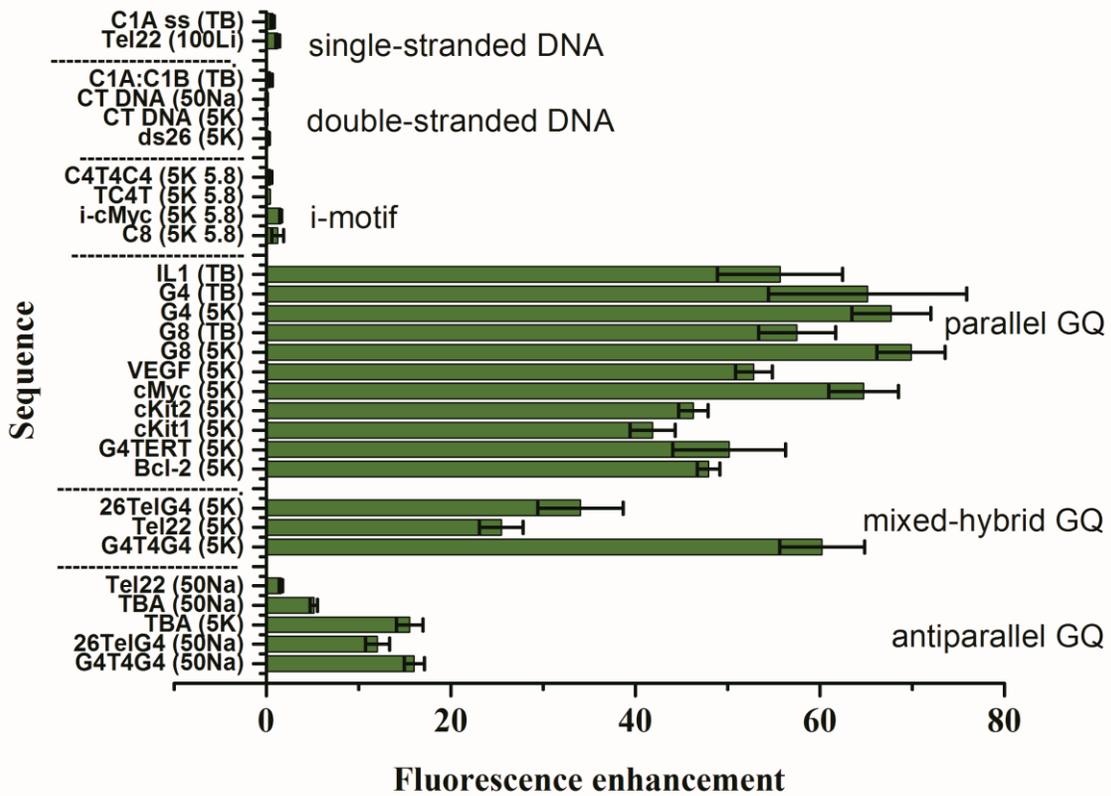
Fig. 3. Summary of fluorescence data for NMM incubated with 10-fold molar excess of indicated sequences. Fluorescence enhancement is reported relative to the fluorescence of NMM alone. Error bars are one standard deviation (confidence interval 68.2%).